Front. Phys., 2013, 8(5): 577–584
DOI 10.1007/s11467-013-0372-2

REVIEW ARTICLE

Recent progress of laser driven particle acceleration at Peking University

Xue-Qing Yan†, Chen Lin, Hai-Yang Lu, Kun Zhu, Yu-Bin Zou, Hong-Yong Wang, Bing Liu, Shuan Zhao, Jiao Zhu, Yi-Xing Geng, He-Zheng Fu, Yong Shang, Chao Cao, Yin-Ren Shou, Wei Song, Yuan-Rong Lu, Zhong-Xi Yuan, Zhi-Yu Guo, Xian-Tu He, Jia-Er Chen

State Key Laboratory of Nuclear Physics and Technology and CAPT, Peking University, Beijing 100871, China

Corresponding author. E-mail: †x.yan@pku.edu.cn

Received July 26, 2013; accepted August 6, 2013

Recently, radiation pressure acceleration (RPA) has been proposed and extensively studied, which shows that circularly polarized (CP) laser pulses can accelerate mono-energetic ion bunches in a phase-stable-acceleration (PSA) way from ultrathin foils. It is found that self-organizing proton beam can be stably accelerated to GeV in the interaction of a CP laser with a planar target at 10^{22} W/cm^2. A project called Compact LAser Plasma proton Accelerator (CLAPA) is approved by MOST in China recently. A prototype of laser driven proton accelerator (1 to 15 MeV/1 Hz) based on the PSA mechanism and plasma lens is going to be built at Peking University in the next five years. It will be upgraded to 200 MeV later for applications such as cancer therapy, plasma imaging and fast ignition for inertial confine fusion.

Keywords phase-stable acceleration (PSA), laser, ion acceleration, ignition

PACS numbers 52.38.Kd, 41.75.Jv, 52.35.Mw, 52.59.-f

Contents

1 Phase-stable-acceleration

State-of-the-art lasers can deliver ultraintense, ultrashort laser pulses, with intensities exceeding 10^{21} W/cm^2 and very high contrast ratios, in excess of 10^{10}:1. These systems can avoid the formation of plasma by the prepulse, thus opening the way to laser-solid interactions with ultra-thin solid targets [1, 2]. Solid targets irradiated by a short pulse laser can be an efficient and flexible source of MeV protons as well as highly charged MeV ions. Such proton beams are already applied to produce high-energy density matter [3] or applied to radiograph transient processes [4], and they offer promising prospects for tumor therapy [5], isotope generation for positron emission tomography [6], and fast ignition of fusion cores [7].

In the intense-laser interaction with solid foils, usually there are three groups of accelerated ions. The first two occur at the front surface, moving backward and forward, respectively, and the third one is sheath acceleration (TNSA) that occurs at the rear surface [8–10]. As these output beams are accelerated only by electrostatic fields and have no longitudinal bunching in (x, p_x) plane, their distribution profiles used to be exponential nearly with 100% energy spread. Although some techniques can be used to decrease the energy spread, however, they rely on relatively complicated target fabrication [11–13]. Recently, radiation pressure acceleration (RPA) has been proposed and extensively studied, which shows that ultra-intense laser pulses can accelerate mono-energetic ion bunches in a phase-stable-acceleration (PSA) way from ultrathin foils [14–25]. In these surface acceleration mechanisms, the linear polarized (LP) laser pulse is used and the $J \times B$ heating [14] is efficient to generate the hot electrons. For a circu-

Frontiers of Physics

larly polarized (CP) laser pulse with the electrical field $E_L = E(x)[\sin(\omega_L t)\boldsymbol{z} + \cos(\omega_L t)\boldsymbol{z}]$, however, the ponderomotive force is $\boldsymbol{f}_p = \frac{m_e c^2}{2}\frac{\partial}{\partial x}{a_L}^2(x)\boldsymbol{x}$ and its oscillating part vanishes. Here $a_L(x) = eE/(m_e\omega_L c)$ is the normalized laser amplitude, and m_e, and ω_L are the electron mass, laser frequency and charge, respectively. When a CP laser is normally incident on a thin foil, the electrons are pushed forward steadily by the ponderomotive force. There is a regime of proton acceleration in the interaction of a CP laser with a thin foil in a certain parameter range, where the proton beam is synchronously accelerated and bunched like in a conventional RF linac. The acceleration mechanism is thus named Phase Stable Acceleration (PSA). An analytic model is presented to show the acceleration and bunching processes during the laser interaction.

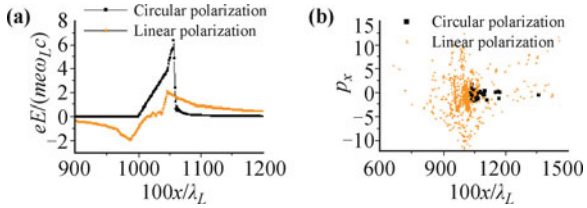

Fig. 1 A thin solid-density target ($n_0/n_c = 10$, $D = 0.2\lambda_L$) is irradiated by a short laser pulse with a normalized laser amplitude $a_L = 5$. **(a)** Electrostatic field, **(b)** Electron phase space (x, p_x) distribution. Reproduced from Ref. [28].

As the oscillating part of the ponderomotive force is zero for CP laser pulse and $J \times B$ heating does not work, the interaction process is completely different from LP case. Figure 1 shows the electrical field profile and phase space projections for both circular and linear polarizations. In LP case, electrons are obvious heated by $J \times B$ force and randomly distributed in the space. The charge separation field is many times smaller than in CP case [see Fig. 1(a)]. In contrast, the electrons are quickly pushed inward by the ponderomotive force of the CP laser pulse, so that they pile up in the front of laser pulse and make up of a compressed electron layer.

In order to discuss the PSA regime easily, a simple model can be derived to elucidate the bunch formation for laser plasma interaction [21, 28]. A linear profile of both in the electron depletion region ($E_{x1} = E_0 x/d$ for $0 < x < d$) and in the compressed electron layer ($E_{x2} = E_0[1-(x-d)/l_s]$ for $d < x < d+l_s$) can be seen in Fig. 2. The parameter E_0, n_{p0} and l_s are related by the equations $E_0 = 4\pi end$ and $n_{p0} l_s = nd \approx n_0 d$. As the E_{x1} increases with x, the protons starting at initial positions $x < d$ are debunched (longitudinally defocused) and their density will decrease in the electron depletion region. On the contrary, because the E_{x2} decreases with x, the protons inside the compression layer ($d < x < d+l_s$) can be bunched by the electrostatic field E_{x2}. The equilibrium between the electrostatic and the ponderomotive forces on electrons is only transitorily lost and the electrons rearrange themselves quickly to provide a new equilibrium if the laser pulse is not over. So the light pressure exerted on the electrons $(1+\eta)I_L/c$ is assumed to be balanced by the electrostatic pressure $E_0 e n_{p0} l_s/2$. Here η is the reflecting efficiency.

As the purely hydrodynamic description is not adequate to describe the interaction between the protons and electrons, dynamic equations are derived based on this model [28]. We introduce $\xi = (x_i - x_r)$ with $-l_s/2 < \xi < l_s/2$, where $x_r = d + l_s/2$ represents the position for the reference particle. The force acting on a test ion is given by $F_i = q_i E_0[1-(x_i-d)/l_s]$. Thus, the motion equation for the proton is $\frac{\mathrm{d}^2 x_i}{\mathrm{d}t^2} = \frac{q_i E_0}{m_i \gamma^3}[1-(x_i-d)/l_s]$, γ is the relativistic factor for reference particle. The phase motion (ξ, t) can be written as

$$\ddot{\xi} = -\Omega^2 \xi, \quad \Omega^2 = \frac{q_i E_0}{m_i l_s \gamma^3} \tag{1}$$

For the reference ion γ varies slowly and E_0 is assumed to be quasi-constant the longitudinal phase motion (ξ, t) is a harmonic oscillation. We can obtain

$$\xi = \xi_0 \sin(\Omega t) \tag{2}$$

$$\dot{\xi} = -\xi_0 \Omega \cos(\Omega t) \tag{3}$$

If we take the laser amplitude $a_L = 5$, $n_0/n_c = 10$, and $\gamma = 1$ for protons at the beginning, the period of the first longitudinal oscillation is about $8T_L$, which was consistent with the simulation results as shown in Fig. 5. If the final energy of reference particle $W_r = 300$ MeV, then energy spread $\Delta W/W_r = \xi_0 \Omega/W_r$ will be less than 4%.

2 PIC simulation

In order to examine the present model and dynamics process, we carried out one-dimensional (1D) simulations by a fully relativistic PIC simulation code (KLAP) [21, 31] and 100 particles per cell per species, with cell sizes of $\lambda_L/100$. In PIC simulations a laser pulse with $a_L = 5$ and duration $100T_L$ is incident on a purely hydrogen plasma (cold, step boundary, overdense plasma slab with $n_0/n_c = {\omega_p}^2/{\omega_L}^2 = 10$ and $D = 0.2\lambda_L$) where $n_c = m_e{\omega_L}^2/(4\pi e^2)$ is the critical density, ω_p is the plasma frequency. In simulations the target boundary is located at $x = 10\lambda_L$ and the laser impinges on it at $t = 10T_L$, λ_L and T_L are the laser wavelength and period. The a_L is the laser field amplitude given in units of the dimensionless parameter, and m_e, ω_L and e are the

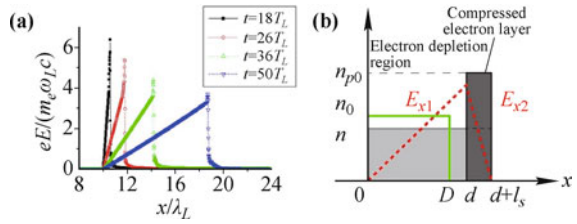

Fig. 2 **(a)** Snapshots of the spatial distributions of the electrostatic fields at different time, where the initial plasma density $n_0/n_c = 10$ and thickness $D = 0.2\lambda_L$, normalized laser peak-amplitude $a_L = 5$ and pulse duration duration $= 100T_L$; **(b)** Schematic of the equilibrium density profiles for ions (n) and electrons (n_{p0}). The x position at $x = d$ indicates the electron front, where the laser evanescence starts and it vanishes at $x = d + l_s$, where l_s is the plasma skin depth. The initial plasma density n_0 and target thickness D are also plotted. Reproduced from Ref. [21].

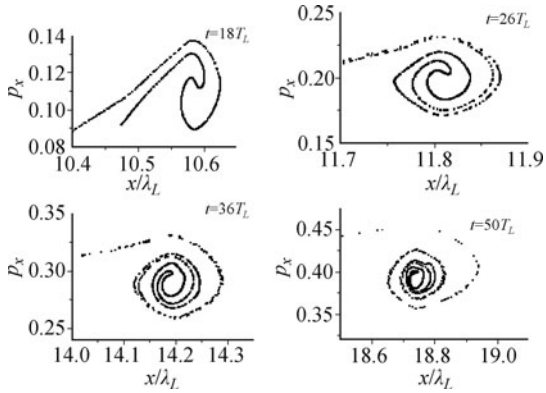

Fig. 3 Evolution of phase space distribution for protons, the 1st, 2nd, 3rd and 4th oscillation period are 18, 26, 36 and 50 T_L respectively. The laser reflection efficiency $\eta = 0.38$. Reproduced from Ref. [21].

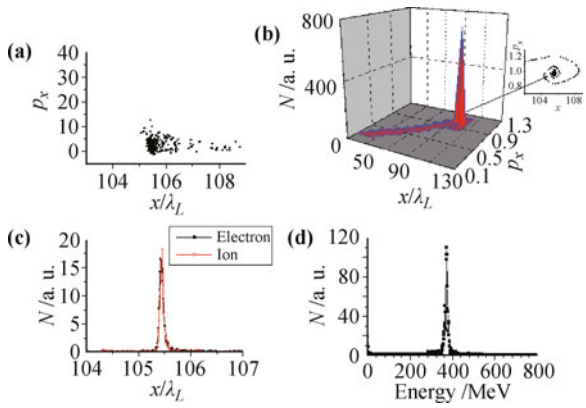

Fig. 4 **(a)** Phase space distribution of electrons; **(b)** Phase space distribution of protons; **(c)** Electrons and protons density profiles; **(d)** Energy spectrum of protons. The results are found at $t = 200T_L$ when the laser interaction is almost terminated. The laser and plasma parameters are the same as in Fig. 1. Reproduced from Ref. [21].

electron mass, laser frequency and charge, respectively.

The snapshots of the electrostatic field profile in Fig. 2(a) shows that the depletion region expands with time and the proton density in this region decreases, so that the slope of the field in the depletion region reduces gradually. In the compressed electron layer, it is found that the width of the compression layer remains to be equal to the skin depth ($l_s \approx \lambda_L/20$). Therefore the charge separation field in this layer nearly keeps the same steep linear profile, even though the maximum separation field is decreased slightly. It means the protons in the compressed electron layer can be synchronously accelerated and bunched by the charge separation field, so that the phase oscillations appear in the proton phase space (see Fig. 3), which is quite similar with the radio frequency accelerator.

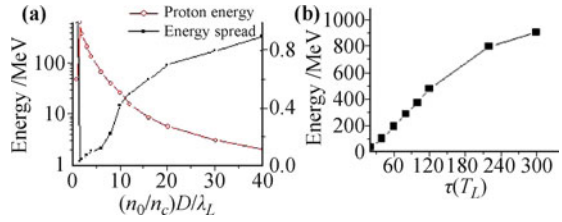

Fig. 5 **(a)** Proton energy of the mono-energetic peak versus target thickness and density for $a_L = 5$ and laser pulse duration $=100\ T_L$; **(b)** Proton energy of the mono-energetic peak versus laser pulse duration for $a_L = 5$, $n_0/n_c = 10$, and $D = 0.2\lambda_L$. Reproduced from Ref. [21].

The snapshots of phase-space distributions of electrons and ions at $t = 200T_L$ are plotted in Figs. 4(a) and (b). It shows that a bunched proton beam with a very high density is formed in the phase space (x, p_x), because protons inside the compressed electron layer always execute periodical oscillations as described by Eq. (3). The protons in the electron depletion region (between $x = 0$ and 100) are debunched and form a long tail in the phase space, however, its density is two-orders lower than in the compressed electron layer. As a result, the debunched protons seem to have disappeared in the proton spatial distribution and the proton energy spectrum, which are shown in Figs. 4(c) and (d), respectively. Figure 4(c) implies that both particles have the same density profiles and a quasi-neutral beam is therefore obtained. In this case, the space charge fields are weak and the proton beam can propagate over a long distance without explosion, which is advantageous to transport the high current ion beams in applications. The energetic proton beam has a low FWHM energy spread ($< 4\%$) and high peak current as shown in Fig. 4(d). The energy spread is completely in agreement with our earlier estimation based upon Eq. (3). Note that the proton bunch has an ultrashort length about the skin depth l_s or about 250 attoseconds in time ($\lambda_L = 800$ nm). The number of accelerated protons in the bunch is about $n_0 l_s \theta$, where θ is the focused beam spot area. This gives about quasi-monoenergetic protons for a focused beam diameter of

40 μm in the present simulation.

In 1D simulations it is found that the proton energy depends on the product of target density and thickness. The proton energy and the energy spread are plotted versus the electron area density in Fig. 5(a). It shows that the energy spread can be optimized near the condition $a_L \propto (n_0/n_c)D/\lambda_L$. Figure 5(b) suggests that the proton energy increases almost linearly with the laser pulse duration at first, Later it turns to be saturated because the protons become relativistic.

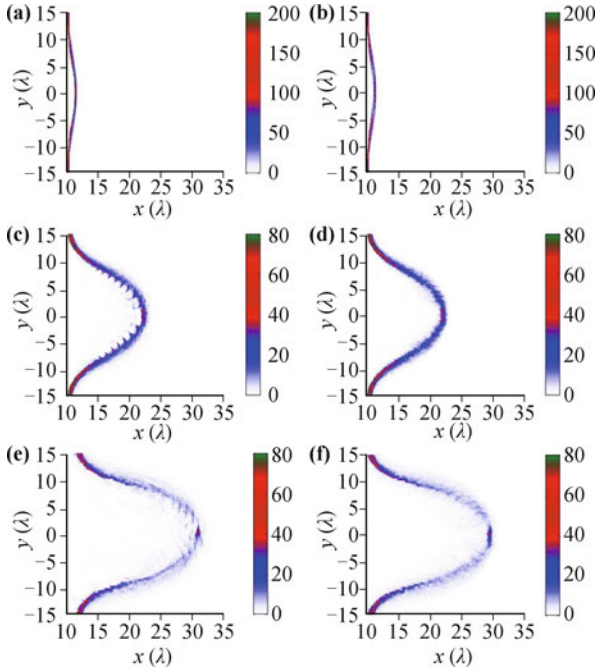

Fig. 6 Foil density evolution. Left: electrons, right: ions, at times **(a, d)** $t = 16$, **(b, e)** $t = 36$, **(c, f)** $t = 46$, in units of laser period. The laser pulse is incident from the left and hits the plasma at $t = 10$. Only half the transverse size of the simulation box is plotted in frames (b), (c), (e), (f) for better resolution of fine structures. Here $a_L = 50$ and pulse duration is $30T_L$. Reproduced from Ref. [26].

For appropriate parameters, CP pulses may accelerate foils as a whole with most of the transferred energy carried by ions. The basic dynamics are well described by a 1D PSA model. Acceleration terminates due to multi-dimensional effects such as transverse expansion of the accelerated ion bunch and transverse instabilities. In particular, instabilities grow in the wings of the indented foil, where light is obliquely incident and strong electron heating sets in. Eventually, this part of the foil is diluted and becomes transparent to the driving laser light. The central new observation in the present paper is that this process of foil dispersion may stop before reaching the centre of the focal spot and that a relatively stable ion clump forms near the laser axis which is efficiently accelerated. The dense clump is about 1–2 laser wavelengths in diameter. The stabilization is related to the driving laser pulse that has passed the dispersed foil in the transparent wing region and starts to encompass the opaque clump, keeping it together (see Fig. 6).

Figure 7 highlights the central results concerning clump evolution. The total number of protons, comprised within a $\lambda_L/2$ distance from the laser axis and shown in Fig. 7(a), drops after time $t = 26$ from an initial value of 2.5×10^{10} due to transverse expansion, but this trend is interrupted at about $t = 35$, when the foil becomes transparent in the wing region and the new regime of quasi-stable acceleration sets in. In the present 2D-PIC simulation, about 1.7×10^{10} protons (1 nano-Coulomb) are trapped in the central clump and are accelerated to an ion energy of approximately 1 GeV. The ion energy spectra exhibit sharp peaks, as it is seen in Fig. 7(b).

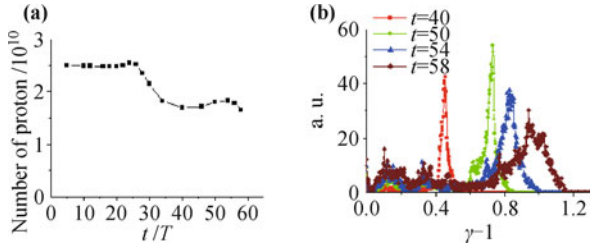

Fig. 7 **(a)** Number of protons in the center of the foil ($r < \lambda_L$) versus time in units of laser cycles; **(b)** Evolution of energy spectrum for beam ions located inside the central clump ($r < \lambda_L$). Reproduced from Ref. [26].

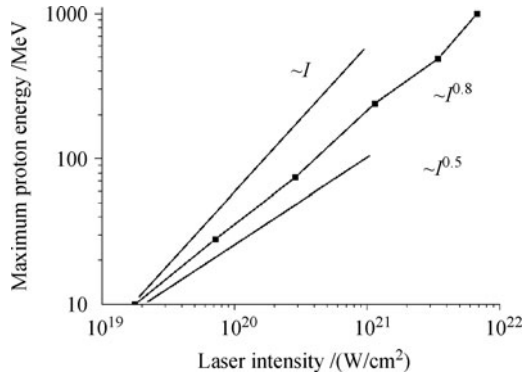

Fig. 8 Proton energy versus laser intensity. Reproduced from Ref. [36].

Maximum proton energy versus laser intensity is plotted in Fig. 8. The black squares represent results from the 2D-PIC simulations described below. They follow an effective scaling of $I^{0.8}$.

3 Proof of principle experiment

There were successful experimental demonstration on ion

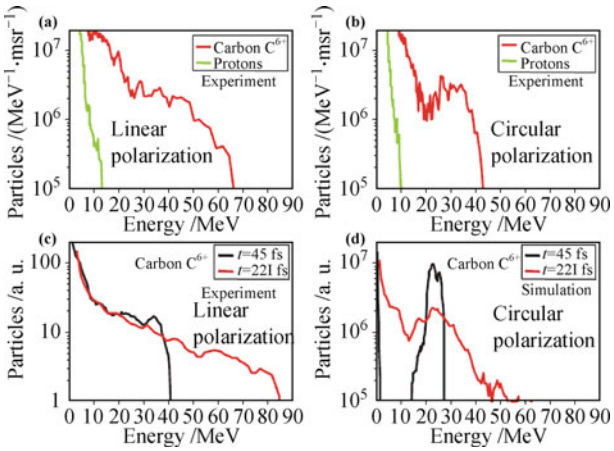

Fig. 9 Experimentally observed proton (*green curves*) and carbon C^{6+} (*red curves*) spectra in the case of linear **(a)** and circular **(b)** polarized irradiation of a 5.3 nm thickness DLC foil. The corresponding curves as obtained from 2D PIC simulations **(c)**, **(d)** show excellent agreement with the measured distributions at late times. Reproduced from Ref. [29].

acceleration from ultrathin diamond like carbon foils (DLC) irradiated by ultrahigh contrast laser pulses of energy 0.7 J focused to peak intensities of 5×10^{19} W/cm^2 [29]. A reduction in electron heating is observed when the laser polarization is changed from linear to circular, leading to a pronounced peak in the fully ionized carbon spectrum at the optimum foil thickness of 5.3 nm as shown in Fig. 8. 2D particle-in-cell simulations reveal that those C^{6+} ions are for the first time dominantly accelerated in a phase-stable way by the laser radiation pressure.

4 Laser plasma lens

In principle higher proton energy (for example, GeV) can be realized by using a higher laser intensity, however, in order to accelerate ions to a relativistic velocity, hole-boring effects and transverse instabilities should be restrained, which normally require extremely high laser intensity ($> 10^{21}$ W/cm^2), sharp rising front, and high temporal laser contrast ($> 10^{10}$), which are very challenging for state of art laser technology. We propose a plasma lens to make high intensity, high contrast laser pulses with a steep front (see Fig. 10). When an intense, short Gaussian laser pulse pass through nearly critical dense plasma, the laser pulse will be compressed and focused into a channel due to self-focusing and self-modulation. If it is used as a plasma lens, three pulse shaping effects are realized synchronously: i) pulse focusing that results in laser intensity enhancement; ii) laser profile steepening; iii) absorption of non- relativistic prepulse. The transmission efficiency of the lens can be as high as 60% and it will be useful for many applications such as generation of high-energy ions and electrons.

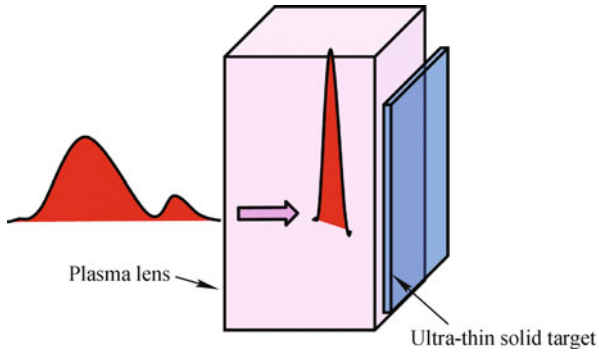

Fig. 10 Laser plasma lens for pulse shaping and cleaning.

5 Self-matching resonance acceleration

In the critical dense plasma there is a novel self-matching resonance acceleration (SMRA) regime for generating dense relativistic electron beams by using ultraintense circularly-polarized laser pulses in near-critical density plasmas [32]. Under these conditions, the self-generated quasistatic magnetic fields (both azimuthal and axial) play an important role. When the self-generated quasistatic axial magnetic field is strong enough to pinch and trap thermal relativistic electrons, an overdense electron bunch is trapped and formed in the center of the laser channel as shown in Fig. 11.

In combination of the self-generated magnetic fields (both in axial and azimuthal direction) and the laser pulse, relativistic electrons can experience two processes: in the trapping process, the electron betatron frequencies and phases are adjusted automatically to match the resonance conditions; in the resonance process, the matched electrons are accelerated continuously along the laser propagation direction. All resonance electrons show similar dynamic behavior, which can be explained by the SMRA model, in which a collimated relativistic electron beam with overcritical density, helical structure, and plateau profile energy spectrum, can be generated. This experiment might be very promising for MeV hard photon (X/γ ray) production or ion acceleration.

The energy spectrum of electrons for the LP laser case shows a thermal-like distribution due to lack of the axial magnetic field, while the angular distribution of electron energy for the LP laser case shows a larger divergence angle and a lower energy peak.

6 Target fabrication

In order to realize Phase Stable Acceleration of ions, it

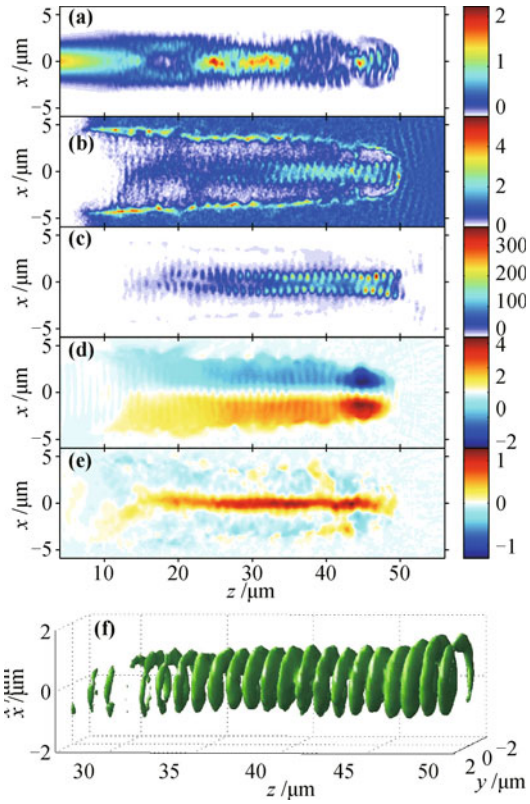

Fig. 11 Simulation results at $t = 80$ T. **(a)**–**(e)** Longitudinal (Z, X) cuts along the pulse axis of, (a) instantaneous laser intensity I, normalized by the initial intensity; **(b)** electron density n_e, normalized by the critical density n_c; **(c)** electron energy density; **(d, e)** self-generated azimuthal and axial magnetic fields B_S and B_{S_z}, averaged over laser period. **(f)** 3D isosurface distribution of electron energy density. Reproduced from Ref. [32].

is necessary to have free-standing nanometer-thickness target [29]. By using the filtered cathodic vacuum arc system, we have successfully manufactured free standing, diamond-like-carbon (DLC) films. The foil thickness can be accurately controlled by the arc counts as Fig. 12 shows. The thickness of films has been characterized by atomic force microscope. Figure 13 is a 5 nm DLC foil coated on Si substrate.

7 Proton acceleration from two layer targets

A novel efficient and stable mechanism has been designed to generate 200 MeV proton bunch by irradiating a two-layer targets (near-critical density layer+solid density layer with heavy ions and protons) with a p-polarized Gaussian pulse at intensity of 10^{20} W/cm^2 (see Fig. 14). The laser intensity is enhanced by the laser self-focusing effect in the near-critical density layer. Meanwhile the electrons are efficiently accelerated in the laser propagation direction by the direct laser acceleration. It is further found that when the self-generated quasistatic axial

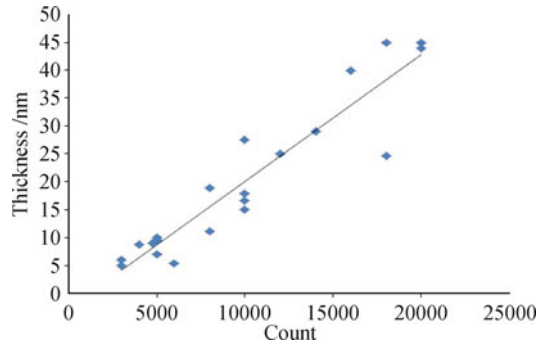

Fig. 12 DLC film thickness versus arc counts. Reproduced from Ref. [31].

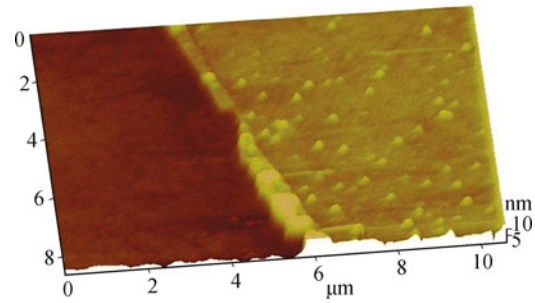

Fig. 13 AFM image of DLC coated on Si substrate. Reproduced from Ref. [36].

magnetic field is strong enough to pinch and trap the thermal relativistic electrons, an overdense electron bunch can appear in the center of the plasma channel produced by the laser pulse. In the case of CP laser pulse a collimated relativistic electron beam with over-critical density and helical structure is generated [32]. A stronger sheath field is hence built up at the rear side of the solid density layer by the combination interaction of the shaped laser pulse and the energetic electrons, leading to more efficient and stable proton acceleration. Compared to a single-layer solid target, Fig. 15 implies the proton peak energy is increased by a factor of three and the energy spread is remarkably decreased from the two-layer target [33–35].

8 CLAPA project at Peking University

A project called Compact LAser Plasma proton Accelerator (CLAPA) is approved by MOST in China recently. A prototype of laser driven proton accelerator (1∼15 MeV/1 Hz) based on the PSA mechanism and plasma lens will be built at Peking University in the upcoming five years (see Fig. 16). It will be upgraded to hundreds of MeV proton later for the applications such as cancer therapy, plasma imaging and fast ignition for inertial confine fusion.

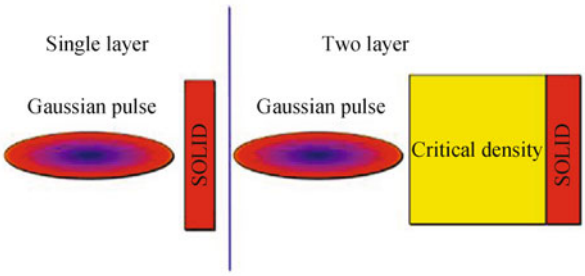

Fig. 14 From single nanometer target to two layer target.

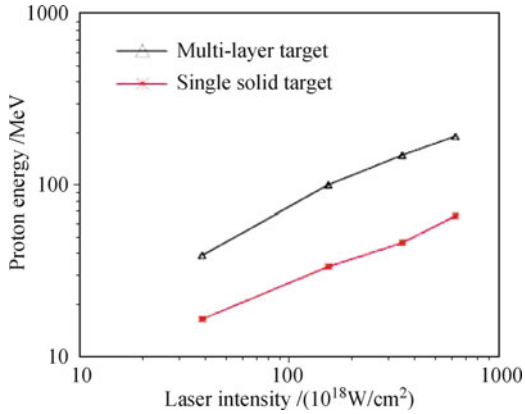

Fig. 15 Parameter scanning for proton energy scaling law Energy scaling for two-layer target with fixed near-critical plasma skin length and single-layer solid target. Reproduced from Refs. [33, 34].

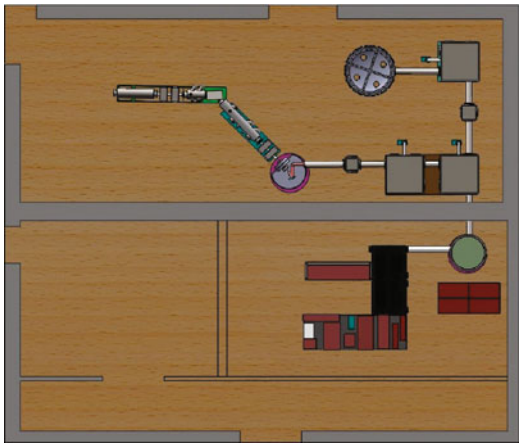

Fig. 16 Compact LAser Plasma proton Accelerator (CLAPA) at Peking University.

Acknowledgements This work was supported by National Basic Research Program of China (Grant No. 2013CBA01502), National Natural Science Foundation of China (Grant Nos. 11025523, 10935002, 10835003, and J1103206), and National Grand Instrument Projetc (2012YQ030142). The authors acknowledge stimulating discussions with Prof. MtV and Prof. Z. M. Sheng.

References

1. G. A. Mourou, T. Tajima, and S. V. Bulanov, Optics in the relativistic regime, *Rev. Mod. Phys.*, 2006, 78(2): 309
2. A. Mackinnon, Y. Sentoku, P. Patel, D. Price, S. Hatchett, M. Key, C. Andersen, R. Snavely, and R. Freeman, Enhancement of proton acceleration by hot-electron recirculation in thin foils irradiated by ultraintense laser pulses, *Phys. Rev. Lett.*, 2002, 88(21): 215006
3. P. Patel, A. Mackinnon, M. Key, T. Cowan, M. Foord, M. Allen, D. Price, H. Ruhl, P. Springer, and R. Stephens, Isochoric heating of solid-density matter with an ultrafast proton beam, *Phys. Rev. Lett.*, 2003, 91(12): 125004
4. M. Borghesi, D. H. Campbell, A. Schiavi, M. G. Haines, O. Willi, A. J. MacKinnon, P. Patel, L. A. Gizzi, M. Galimberti, R. J. Clarke, F. Pegoraro, H. Ruhl, and S. Bulanov, Electric field detection in laser-plasma interaction experiments via the proton imaging technique, *Phys. Plasmas*, 2002, 9(5): 2214
5. S. V. Bulanov, T. Zh. Esirkepov, V. S. Khoroshkov, A. V. Kuznetsov, and F. Pegoraro, Oncological hadrontherapy with laser ion accelerators, *Phys. Lett. A*, 2002, 299(2–3): 240
6. I. Spencer, K. W. D. Ledingham, R. P. Singhal, T. McCanny, P. McKenna, E. L. Clark, K. Krushelnick, M. Zepf, F. N. Beg, M. Tatarakis, A. E. Dangor, P. A. Norreys, R. J. Clarke, R. M. Allott, and I. N. Ross, Laser generation of proton beams for the production of short-lived positron emitting radioisotopes, *Nucl. Instrum. Methods B*, 2001, 183(3–4): 449
7. M. Roth, T. Cowan, M. Key, S. Hatchett, C. Brown, W. Fountain, J. Johnson, D. Pennington, R. Snavely, S. Wilks, K. Yasuike, H. Ruhl, F. Pegoraro, S. Bulanov, E. Campbell, M. Perry, and H. Powell, Fast ignition by intense laser-accelerated proton beams, *Phys. Rev. Lett.*, 2001, 86(3): 436
8. P. Mora, Plasma expansion into a vacuum, *Phys. Rev. Lett.*, 2003, 90(18): 185002
9. T. Esirkepov, M. Yamagiwa, and T. Tajima, Laser ion-acceleration scaling laws seen in multiparametric particle-in-cell simulations, *Phys. Rev. Lett.*, 2006, 96(10): 105001
10. Y. T. Li, Z. M. Sheng, Y. Ma, Z. Jin, J. Zhang, Z. Chen, R. Kodama, T. Matsuoka, M. Tampo, K. Tanaka, T. Tsutsumi, T. Yabuuchi, K. Du, H. Zhang, L. Zhang, and Y. Tang, Demonstration of bulk acceleration of ions in ultraintense laser interactions with low-density foams, *Phy. Rev. E*, 2005, 72(6): 066404
11. H. Schwoerer, S. Pfotenhauer, O. Jäckel, K. U. Amthor, B. Liesfeld, W. Ziegler, R. Sauerbrey, K. W. D. Ledingham, and T. Esirkepov, Laser-plasma acceleration of quasi-monoenergetic protons from microstructured targets, *Nature*, 2006, 439(7075): 445
12. T. Toncian, et al., Ultrafast laser-driven microlens to focus and energy-select mega-electron volt protons, *Science*, 2006, 312(5772): 410
13. M. Hegelich, B. J. Albright, J. Cobble, K. Flippo, S. Letzring, M. Paffett, H. Ruhl, J. Schreiber, R. K. Schulze, and J. C. Fernández, Laser acceleration of quasi-monoenergetic MeV ion beams, *Nature*, 2006, 439(7075): 441

14. W. L. Kruer and K. Estabrook, $J \times B$ heating by very intense laser light, *Phys. Fluids*, 1985, 28(1): 430
15. A. Macchi, F. Cattani, T. V. Liseykina, and F. Cornolti, Laser acceleration of ion bunches at the front surface of overdense plasmas, *Phys. Rev. Lett.*, 2005, 94(16): 165003
16. S. G. Rykovanov, J. Schreiber, J. Meyer-ter-Vehn, C. Bellei, A. Henig, H. C. Wu, and M. Geissler, Ion acceleration with ultra-thin foils using elliptically polarized laser pulses, *New J. Phys.*, 2008, 10(11): 113005
17. X. Zhang, B. Shen, X. Li, Z. Jin, F. Wang, and M. Wen, Efficient GeV ion generation by ultraintense circularly polarized laser pulse, *Phys. Plasmas*, 2007, 14(12): 123108
18. C. S. Liu, V. K. Tripathi, and X. Shao, Frontiers in modern plasma physics, *AIP Conf. Proc.* , 2008, 1061: 246
19. B. Qiao, M. Zepf, M. Borghesi, and M. Geissler, Stable GeV ion-beam acceleration from thin foils by circularly polarized laser pulses, *Phys. Rev. Lett.*, 2009, 102(14): 145002
20. O. Klimo, J. Psikal, J. Limpouch, and V. T. Tikhonchuk, Monoenergetic ion beams from ultrathin foils irradiated by ultrahigh-contrast circularly polarized laser pulses, *Phys. Rev. ST Accel. Beams*, 2008, 11(3): 031301
21. X. Q. Yan, C. Lin, Z. Sheng, Z. Guo, B. Liu, Y. Lu, J. Fang, and J. Chen, Generating high-current monoenergetic proton beams by a circularlypolarized laser pulse in the phase-stable acceleration regime, *Phys. Rev. Lett.*, 2008, 100(13): 135003
22. A. P. L. Robinson, M. Zepf, S. Kar, R. G. Evans, and C. Bellei, Radiation pressure acceleration of thin foils with circularly polarized laser pulses, *New J. Phys.*, 2008, 10(1): 013021
23. M. Chen, A. Pukhov, Z. M. Sheng, and X. Q. Yan, Laser mode effects on the ion acceleration during circularly polarized laser pulse interaction with foil targets, *Phys. Plasmas*, 2008, 15(11): 113103
24. Y. Yin, W. Yu, M. Y. Yu, A. Lei, X. Yang, H. Xu, and V. K. Senecha, Influence of target thickness on the generation of high-density ion bunches by ultrashort circularly polarized laser pulses, *Phys. Plasmas*, 2008, 15(9): 093106
25. T. Esirkepov, M. Borghesi, S. V. Bulanov, G. Mourou, and T. Tajima, Highly efficient relativistic-ion generation in the laser-piston regime, *Phys. Rev. Lett.*, 2004, 92(17): 175003
26. X. Q. Yan, H. Wu, Z. Sheng, J. Chen, and J. Meyer-ter-Vehn, Self-organizing GeV, nanocoulomb, collimated proton beam from laser foil interaction at 7×10^{21} W/cm^2, *Phys. Rev. Lett.*, 2009, 103(13): 135001
27. X. Q. Yan, M. Chen, Z. M. Sheng, and J. E. Chen, Self-induced magnetic focusing of proton beams by Weibel-like instability in the laser foil-plasma interactions, *Phys. Plasmas*, 2009, 16(4): 044501
28. B. C. Liu, Z. H. He, X. Q. Yan, Z. M. Sheng, Z. Y. Guo, Y. R. Lu, and J. E. Chen, Generation of high-current proton beams with a low energy spread by phase-stable acceleration (PSA), *IEEE Trans. Plasma Sci.*, 2008, 36(4): 1854
29. A. Henig, S. Steinke, M. Schnürer, T. Sokollik, R. Hörlein, D. Kiefer, D. Jung, J. Schreiber, B. M. Hegelich, X. Q. Yan, J. Meyer-ter-Vehn, T. Tajima, P. V. Nickles, W. Sandner, and D. Habs, Radiation-pressure acceleration of ion beams driven by circularly polarized laser pulses, *Phys. Rev. Lett.*, 2009, 103(24): 245003
30. H. Y. Wang, C. Lin, Z. M. Sheng, B. Liu, S. Zhao, Z. Y. Guo, Y. R. Lu, X. T. He, J. E. Chen, and X. Q. Yan, Laser shaping of a relativistic intense, short gaussian pulse by a plasma lens, *Phys. Rev. Lett.*, 2011, 107(26): 265002
31. J. Zhu, H. Z. Fu, C. Lin, Y. Gao, S. Zhao, K. Zhu, Y. R. Lu, J. E. Chen, and X. Q. Yan, Preparation of ultra-thin DLC target for laser ion acceleration, *High Power Laser and Particle Beams*, 2013, 25(7): 1723
32. B. Liu, H. Y. Wang, J. Liu, L. B. Fu, Y. J. Xu, X. Q. Yan, and X. T. He, Generating overcritical dense relativistic electron beams via self-matching resonance acceleration, *Phys. Rev. Lett.*, 2013, 110(4): 045002
33. H. Y. Wang, X. Q. Yan, J. E. Chen, X. T. He, W. J. Ma, J. H. Bin, J. Schreiber, T. Tajima, and D. Habs, Efficient and stable proton acceleration by irradiating a two-layer target with a linearly polarized laser pulse, *Phys. Plasmas*, 2013, 20(1): 013101
34. H. Y. Wang, C. Lin, F. L. Zheng, Y. R. Lu, Z. Y. Guo, X. T. He, J. E. Chen, and X. Q. Yan, High-quality proton bunch from laser interaction with a gas-filled cone target, *Phys. Plasmas*, 2011, 18(9): 093105
35. L. Y. Gao, H. Wang, C. Lin, Y. Zou, and X. Yan, Efficient proton beam generation from a foam-carbon foil target using an intense circularly polarized laser, *Phys. Plasmas*, 2012, 19(8): 083107
36. I. Hofmann, J. Meyer-ter-Vehn, X. Q. Yan, A. Orzhekhovskaya, and S. Yaramyshev, Collection and focusing of laser accelerated ion beams for therapy applications, *Phys. Rev. ST Accel. Beams*, 2011, 14(3): 031304